Lab on a Chip

Cite this: *Lab Chip*, 2011, **11**, 4006

www.rsc.org/loc

PAPER

Strong enhancement of streaming current power by application of two phase flow

Yanbo Xie,[a] John D. Sherwood,[b] Lingling Shui,[a] Albert van den Berg[a] and Jan C. T. Eijkel[a]

Received 17th May 2011, Accepted 30th September 2011
DOI: 10.1039/c1lc20423h

We show that the performance of a streaming-potential based microfluidic energy conversion system can be strongly enhanced by the use of two phase flow. Injection of gas bubbles into a liquid-filled channel increases both the maximum output power and the energy conversion efficiency. In single-phase systems the internal conduction current induced by the streaming potential limits the output power, whereas in a two-phase system the bubbles reduce this current and increase the power. In our system the addition of bubbles enhanced the maximum output power of the system by a factor of 74 and the efficiency of the system by a factor of 163 compared with single phase flow.

Introduction

Energy has become an important topic in scientific research. In particular, novel environmentally-friendly energy conversion systems are required. The developing "lab on a chip" technology provides new opportunities to convert fluidic mechanical energy to electrical energy.[1]

Electro-kinetic phenomena, such as electro-osmotic flow and streaming current, convert electrical energy into mechanical energy or vice-versa.[2] In this paper we consider the use of streaming potentials to convert mechanical energy into electrical energy. Most solid surfaces in contact with an aqueous solution become electrically charged, due to the dissociation of charged groups on the surface. This leads to the formation of an electrical double layer (EDL) consisting of the charged surface together with a diffuse cloud of mobile counter-ions in the adjacent fluid. If we apply an external pressure difference between the ends of a liquid-filled channel, the mobile ions move with the flowing liquid, thereby creating an electrical current. By placing electrodes at the two ends of the channel, we can capture the electrical energy. As a result, mechanical energy can be converted into electrical energy in a straightforward and effective manner. This is the converse of electro-osmosis, in which an imposed electric field generates fluid motion.

In the past, investigators have studied the performance of such fluidic energy conversion systems using single phase (water) flow.[3] Yang *et al.*[4] noted that the streaming current in fluidic channels could be a simple and effective energy conversion system, but in the examples they considered the energy conversion efficiency was less than 0.05%. Subsequently many researchers have tried to enhance the energy conversion efficiency by using nano-channels with EDL overlap, and efficiency has reached about 3 to 5% in single nano-channels[5] and nanopores[6] respectively. Recently, Duffin and Saykally[7,8] used microjets to enhance the energy conversion efficiency to above 10%.

Streaming currents or potentials generated by multiphase flow have been studied for geophysical, mineral and petroleum applications involving large length scales.[9–12] In this paper, we investigate the effect of two-phase flow on energy conversion at the microscopic scale, and show that the injection of bubbles into a liquid channel strongly increases both the maximum output power and the conversion efficiency.

Principle

A streaming potential generates both a current I_{ext} through the external circuit, and an internal conduction current I_C flowing in the channel in the opposite direction to the streaming current $I_S = I_{ext} + I_C$ (see Fig.1). In the two-phase flow system, gas bubbles with almost zero conductivity are injected into the moving liquid phase. The gas bubbles occupy most of the cross-sectional area of the channel, leaving little space for ion transport.[13–15] As a consequence the electrical resistance of the channel increases, decreasing I_C and making I_{ext} higher than in single phase flow. As a result, the power delivered to the external circuit increases. At the same time the input power needed to generate the flow is not significantly affected, so that the power conversion efficiency increases. We used one of the simplest ways to generate gas bubbles in our system, namely a T junction (shown in Fig. 1a).

Experimental setup

A gas source (99% purity N_2) was used both to drive the liquid flow and to generate gas bubbles. The gas source was connected to a gas-tight bottle filled with a liquid solution that was forced into a microfluidic chip *via* fused silica tubing (44 cm long, 150 μm ID) (Fig. 1b). The chip outlet was connected to a waste reservoir *via* fused silica

[a]*BIOS lab on chip group, MESA+ Institution of Nanotechnology, University of Twente, The Netherlands*
[b]*Department of Applied Mathematics and Theoretical Physics, University of Cambridge, United Kingdom*

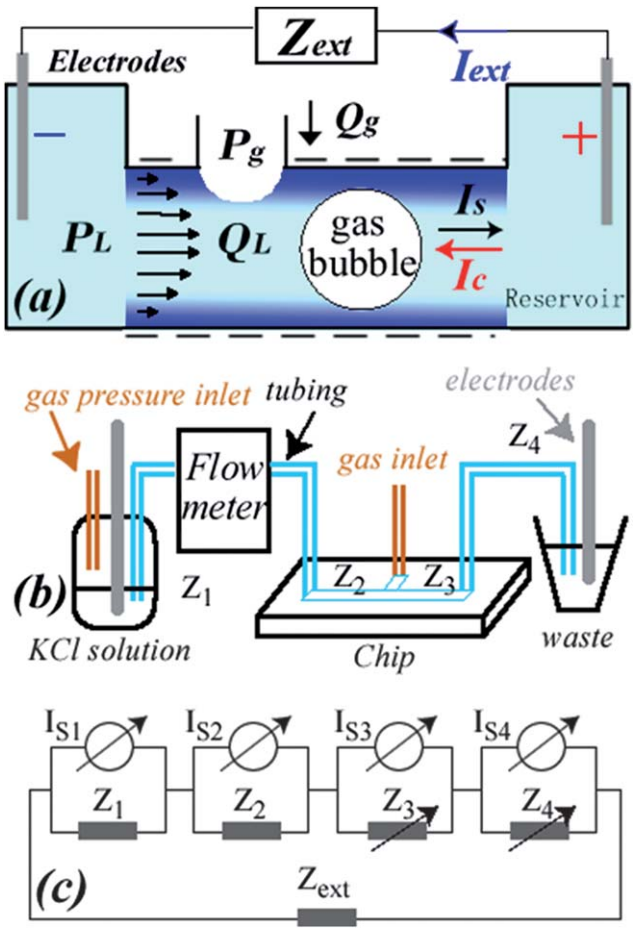

Fig. 1 (a) Schematic of the experiment. (b) The main sections of the experimental setup. (c) The equivalent circuit of the energy generation system, divided into 4 sections. I_{S1} and Z_1 refer to the inlet tubing; I_{S2} and Z_2 to the chip channel before the T junction; I_{S3} and Z_3 to the chip channel after the T-junction and I_{S4} and Z_4 to the outlet tubing.

tubing (15 cm long, 100 μm ID). A flow meter (Fluigent Maesflo) measured the liquid flow rate Q_L. The gas source was furthermore directly connected to the chip in order to generate gas bubbles. The pressures of the two gas paths were controlled individually using a high accuracy gas pressure pump (Fluigent MFCS). The resulting gas/water two-phase flow was collected in the waste bottle. Two Ag/AgCl electrodes inserted into the gas-tight solution bottle and the waste bottle allowed electrical measurements. Voltages were applied by a Keithley 2410 voltage source, and currents were measured by a Keithley 6485 pico-ammeter. A 1mM KCl solution (bulk conductivity $140 \pm 10\mu S\ cm^{-1}$) was prepared from diluted 1M KCl and the pH adjusted to 9.2. Nonionic surfactant Tween 20 at critical micellar concentration (9.23×10^{-5} M) was added to the solution to assure the reliable generation of gas bubbles. A chip with a T junction channel for bubble generation was fabricated by wet etching in borofloat wafers, containing channels of width $w = 40$ μm, height $h = 10$ μm. and length $L = 3.8$ mm with the T junction in the middle.

Equivalent circuit

Suppose that fluid of viscosity η flows along a channel of length L, width w and height h due to a pressure difference ΔP between the ends of the channel. If charge clouds are thin compared to the channel dimensions (w, h), the electrical streaming current generated by convection of the ionic charge cloud adjacent to the charged walls of the channel is

$$I_S = -\varepsilon\varepsilon_0\zeta wh\Delta P/\eta L \quad (1)$$

where ε_0 is the permittivity of free space, ε the relative permittivity of the fluid and ζ the electrical (zeta) potential at the shear plane of the channel walls. The flow circuit, depicted in Fig. 1(b), consists of four different channel sections connected in series, and an equivalent circuit of the energy conversion system is shown in Fig. 1(c). Each section (numbered i) can be considered as a constant current source with an internal electrical resistance Z_i, the latter determined by the channel cross section, length and solution conductivity. The channel system is finally connected in series with the external resistance Z_{ext}. The resistance of the Ag/AgCl electrodes to charge transport is neglected. When gas bubbles are injected into the system, the electrical resistances Z_3, Z_4 after the T junction vary with the volume fraction of gas, and are therefore marked as variable resistors. From Kirchhoff's laws, we obtain the streaming current of the entire system:

$$I_S = \frac{I_{S1}Z_1 + I_{S2}Z_2 + I_{S3}Z_3 + I_{S4}Z_4}{Z_1 + Z_2 + Z_3 + Z_4} \quad (2)$$

If no current flows in the external circuit, the streaming potential of the system can be expressed as:

$$U_S = I_{S1}Z_1 + I_{S2}Z_2 + I_{S3}Z_3 + I_{S4}Z_4 \quad (3)$$

Assuming all of the resistances obey Ohmic laws, the output power attains its maximum value when $Z_{ext} = Z_1 + Z_2 + Z_3 + Z_4$,[16] so that the external current is $I_S/2$ and the output power is

$$P_{O,\max} = \frac{(I_{S1}Z_1 + I_{S2}Z_2 + I_{S3}Z_3 + I_{S4}Z_4)^2}{4(Z_1 + Z_2 + Z_3 + Z_4)} \quad (4)$$

Eqns (2) and (4) indicate that the streaming current and output power of a single section become dominant when its resistance is much larger than that of the other sections. After injection of gas bubbles, Z_3 and Z_4 increase and the streaming current generated in these two sections becomes more important, which will explain our experimental results shown below. Due to the large diameter of the tubing in section 4, the bubbles in this tubing at moderate gas flow rates occupy only a small part of the cross-sectional diameter in the outlet tubing, so that Z_4 changes little. At high gas pressure however, gas bubbles start to fuse to form slugs in the outlet tubing, thereby increasing Z_4. We shall ignore this effect in our theoretical analysis of energy conversion in the chip (section b below), in which Z_4 will be considered constant and equal to its value in single phase flow.

Results and discussion

a. Characterization of the entire system

We maintained a constant inlet liquid pressure $P_L = 1$ bar in the gas-tight bottle connected to the liquid inlet tubing, and gradually increased the gas injection pressure P_g so as to introduce gas bubbles. Snapshots of gas bubbles were taken by a high-speed camera (Photron SA3). The volume of the gas bubbles was seen

to increase with P_g (Fig. 2). From the measured length, frequency and velocity of the gas bubbles, we estimated the gas volumetric flow rate and volume fraction, as discussed below. Since the gas volume fraction varies within the different sections of the system, we first discuss the electro-kinetic behavior of the entire system as a function of the measured gas injection pressure P_g; then in section b we focus upon the chip, and consider the electro-kinetic behavior of 2-phase flow within the chip as a function of the estimated gas volume fraction f_g.

To establish the maximum output power of the system, we performed an *I–V* characterization of the system by applying different voltages against the streaming potential between the electrodes, a procedure equivalent to introducing larger load resistances (see Fig. 3a). When the voltage imposed across the electrodes was zero, the current in the external circuit I_{ext} equaled the streaming current of the system I_S. When the voltage was increased, I_{ext} decreased and the conduction current I_C (in the opposite direction to the streaming current) increased. When the current I_{ext} through the external circuit was reduced to zero, the conduction current balanced the streaming current and the applied voltage equaled the streaming potential U_S. We thus obtained the streaming current I_S, the streaming potential U_S and the electrical resistance $Z_S = Z_1 + Z_2 + Z_3 + Z_4 = U_S/I_S$ of the entire system. The maximum output power then follows from eqn (4). The aim of this paper is to show that Z_S, and consequently $P_{O,max}$, strongly increase following the introduction of bubbles.

At a gas injection pressure $P_g = 600$ mbar no gas bubbles were generated. The streaming current in the resulting single phase flow was measured. The experimental data are shown as solid black squares on Fig. 3b, whereas blue open squares indicate theoretical predictions. Results for single-phase flow indicated that in the solution of Tween 20 non-ionic surfactant the zeta potential on the microchip wall was −40 mV (solid black square and open blue square at $P_g = 600$ mbar). Without surfactant the streaming current measured in 1 mM KCL solution indicates a zeta potential of −60 mV (solid red dot, together with open red triangle at $P_g = 600$ mbar). The presence of Tween 20 thus decreases the zeta potential: a similar tendency has been observed for glass surfaces in soy bean protein[17] and in other non-ionic surfactant solutions.[18] Data points and error bars in Fig. 3(b) indicate averaged values and standard deviations from at least three independent experiments. The streaming current increased slowly with gas inlet pressure for $P_g < 800$ mbar and then more rapidly for $P_g > 800$ mbar. This increase is to be expected by eqn (2): the pressure gradient in the chip is much larger than in the tubing (due to the smaller channel cross-section in the chip), and so the streaming currents I_{S2} and I_{S3} generated in the chip are much larger than I_{S1} and I_{S4} in the tubing. The increase of resistance Z_3 by injection of gas bubbles makes the (high) streaming current in the chip dominant in eqn (2), which leads to the observed streaming current increase of the system. At $P_g = 950$ mbar, I_S was found to oscillate between 100 pA and 2 pA (approximately the values of I_{S3} and I_{S4}). We attribute this to random fusion of gas bubbles, and when P_g reaches 1000 mbar the continuous fusion of gas bubbles causes Z_4 to dominate the electrical resistance of the entire system, so that I_{S4} (1.6 pA theoretically compared with 1.52 pA experimentally in single phase flow) becomes the measured system streaming current according to eqn (2).

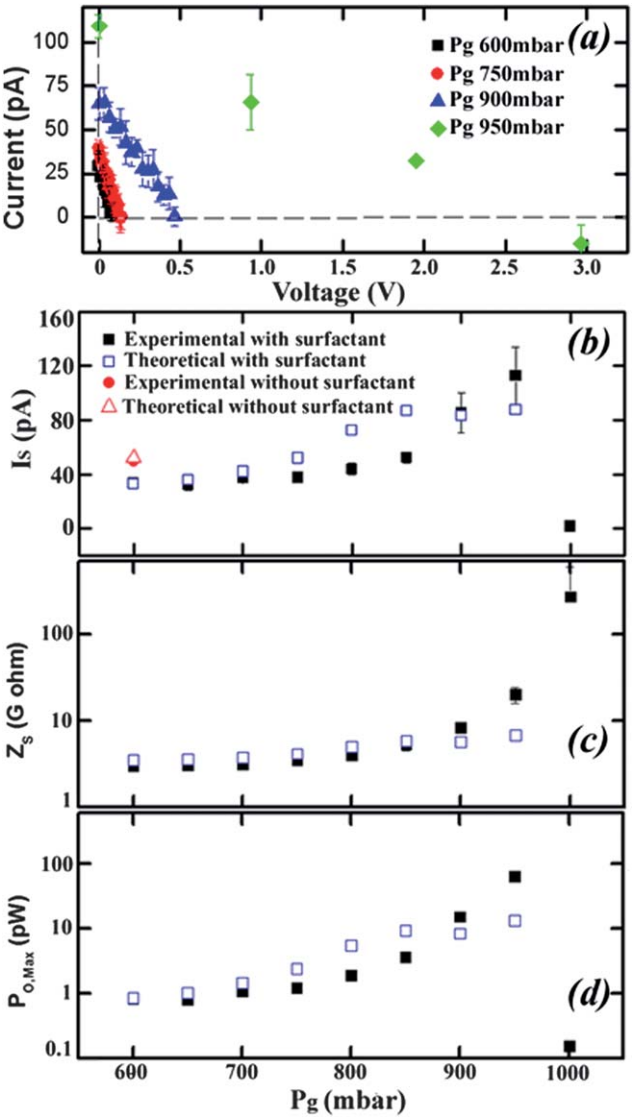

Fig. 3 (a) *I–V* characterization of the system during single-phase water flow (black squares) and two-phase gas/water flow (red, blue, green); (b) streaming current of system as a function of gas injection pressure P_g; (c) electrical resistance of system as a function of P_g; (d) maximum output power of system as a function of P_g. Open blue symbols indicate theoretical values.

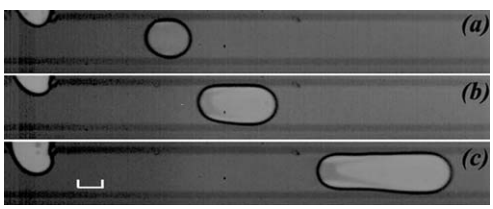

Fig. 2 Gas bubbles injected at gas injection pressure P_g = (a) 650 mbar, (b) 750 mbar, and (c) 900mbar. Bubble volume increases with gas injection pressure. The T junction is located at the top left of each figure. Scale bar in (c) indicates 20μm distance.

The predictions for the streaming current, electrical resistance and output power in Fig. 3 (open blue squares) were obtained as follows. The ΔP over sections 1 and 2, which contain only water, can be predicted from the measured flow rate Q_L and the hydraulic resistance, which for the rectangular channel of section 2 is based on:[20]

$$Q = \frac{\Delta P}{64\eta L}\left\{wh^3\left[\frac{16}{3} - 3.36\frac{h}{w}\left(1 - \frac{h^4}{12w^4}\right)\right]\right\} \quad (5)$$

The streaming current in sections 1 and 2 can then be estimated by eqn (1). We assume that the streaming current generated by 2-phase flow in section 3 is the same as for single phase flow (as suggested by the results of section b below). Assuming that gas bubbles do not coalesce in the outlet tubing, the streaming current in section 4 changes little from that for single phase flow at the new flow rate (and I_{S4} is in any case so small that it has negligible effect in eqn (1)). Changes in the electrical resistance Z_4 of the section are negligible as long as P_g is sufficiently small for gas bubble coalescence not to occur. The electrical resistances Z_1, Z_2 of sections 1 and 2 are unchanged, and the electrical resistance Z_3 of section 3, containing bubbles, is estimated using the bubble dimensions, as discussed in section (b) below. The total electrical resistance Z_S of the system could therefore be predicted from the channel geometry and water conductivity and hence the streaming current of the entire system could be estimated by means of eqn (2). Fig. 3 shows the predicted streaming current, electrical resistance and output power (open blue squares).

The two phase flow electrical resistance Z_S of the entire system was measured, as described above. Fig. 3(c) shows that Z_S strongly increased with gas injection pressure P_g. This is to be expected: as P_g increases, the volume of gas bubbles occupying the liquid channel increases and the conductive area of the channel is reduced. It should be noted that theoretical prediction is smaller than the experimental value at high P_g. This is probably due to fusion of gas bubbles, which form slugs in the outlet tubing as already mentioned above, thereby increasing Z_4.

We conclude that gas bubbles increase both the streaming current and the electrical resistance of the system. The maximum output power can be predicted from eqn (4), using the resistance and streaming current measured when no bubble fusion occurred in section 4. When $P_g = 950$ mbar, $P_{O,max}$ was found to be greater than for single phase flow by a factor of 74.

To calculate the system efficiency, the input power P_{in} was determined as the sum of the gas input power and liquid input power:

$$P_{in} = \sum_i \Delta P_i \cdot Q_i = \Delta P_g \cdot Q_g + \Delta P_L \cdot Q_L \quad (6)$$

The liquid flow rate Q_L was measured by a flow meter; the size and frequency of gas bubbles (and hence the gas flow rate Q_g) could be obtained from hi-speed camera movies. The volume of each gas bubble increased with the gas injection pressure (Fig. 2). At $P_g = 600$ mbar no gas bubbles were generated, and $Q_g = 0$. With increasing gas pressure, the gas flow rate increased, but the presence of gas bubbles led to a reduction in Q_L at constant liquid pressure.[19] Our experimental results indicate that Q_g was much smaller than Q_L, so that the total input power was dominated by the liquid phase according to eqn (6).

Fig. 4(b) shows that the input power gradually decreased with gas injection pressure, being halved at 950 mbar. Also shown is a theoretical prediction of the input power for single phase flow, calculated using eqns (5) and (6).

The energy conversion efficiency (*Eff*) is the ratio of the maximum electrical output power $P_{O,max}$ to the mechanical input power P_{in}:

$$Eff = \frac{P_{O,Max}}{P_{in}} = \frac{I_S^2 Z_S/4}{Q_g P_g + Q_L P_L} \quad (7)$$

The combined effect of increased maximum output power and decreased input power massively enhanced the system energy conversion efficiency by a factor 163 above that for single phase flow (Fig. 5).

b. Characterization of the chip channel

The strong enhancement of the maximum electrical power output for the system as a whole is partly due to the increasing output power of flow section 3 (see Fig. 1) and partly due to the increasing dominance of section 3 in the system efficiency. Both are caused by the introduction of bubbles and the resulting increase of Z_3 (see eqn (4)). Since section 2 of the system (channel before T junction) is occupied only by single phase water, the gas bubbles do not influence its electrical resistance Z_2. The part of the system of greatest theoretical interest therefore is the chip channel past the T-split where bubbles are injected. With suitable assumptions, discussed below, we can determine the increase of output power and efficiency for this section of the system separately. We can thus determine how the maximal output power and efficiency in a microfluidic channel are influenced by two-phase flow.

Electrical resistance increase by two phase flow

Gas bubbles decrease the conductive area of the channel, thereby increasing the channel resistance. To estimate this resistance, we

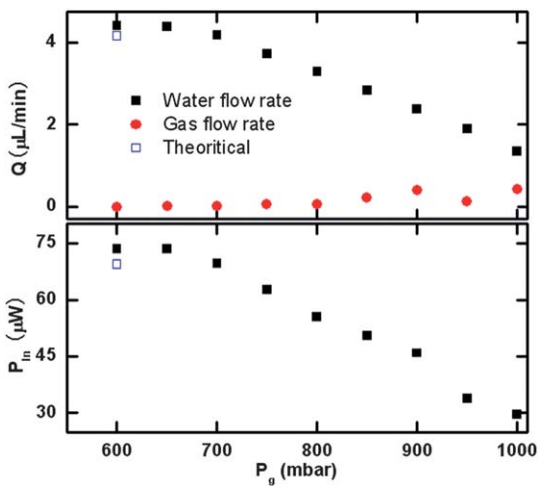

Fig. 4 (a) Gas flow rate Q_g (red) increases with increasing gas volume fraction and liquid flow rate Q_L (black) decreases. (b) The total input power P_{in} (defined by eqn (6)) decreases when gas bubbles are injected into the liquid system.

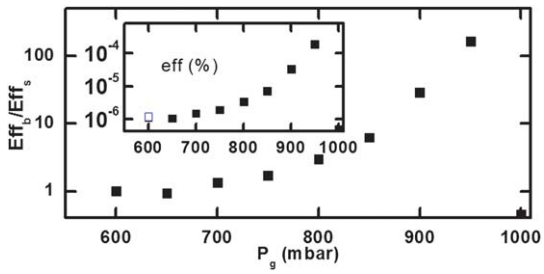

Fig. 5 The efficiency enhancement ratio (ratio of maximum efficiency in two-phase gas/water flow to that in single phase flow (Eff_b/Eff_S)). Inset figure represents the absolute value of the maximum efficiency.

neglect the spherical end-caps of the bubbles, and consider the contribution of the body of the gas bubbles.

A schematic of gas bubble flow in the channel is illustrated in Fig. 6(a) and a cross-sectional view through a bubble is shown in Fig. 6(b). The rectangular cross-section is an approximation of the actual channel shape, which has two corners rounded off as a result of the isotropic etching procedure for manufacturing. The contribution of the liquid film near the wall to the conductive area can be ignored compared with the area of the liquid-filled corners, which was estimated as $h^2(1 - \pi/4)$. From our calculation the conductive area (KCl solution) occupies 5.4% of the total cross-sectional area, which indicates that the resistance Z_b per unit length of a bubble-filled channel will be about 18.6 times the resistance Z_s of the solution-filled channel.

From a movie of gas bubble flow, we measured the length (and hence the average volume) of the gas bubbles close to the T-junction. According to Boyle's law, the gas bubbles expand by a factor approximately 1.5 as they move from the T junction to the channel exit. We therefore assume the average length L_b of the gas bubbles to be a factor 1.25 greater than their length near the T-junction. The average bubble velocity u and generation frequency f were estimated from the movie, and the distance between the leading edges of two consecutive gas bubbles was taken to be u/f. The number of gas bubbles (and liquid slugs of length $L_S = u/f - L_b$) in the channel of length L_3 was therefore $n = L_3 f/u$. We neglect the volume of the bubble spherical end-caps and the liquid volume in the corners, and estimate the gas volume fraction in section 3 as $f_g = nL_b/L_3$. The gas volume fraction in the liquid channel increases with gas injection pressure as shown in Fig. 7. The error bars at higher pressure are caused by increasing variation in the generation process. At low gas injection pressure, the deviation of the bubble dimension is quite small; while at high gas injection pressure, the size variation of gas bubbles becomes larger. We attribute this to the random fusion of gas bubbles in the outlet tubing (section 4), which causes feedback to the generation of gas bubbles *via* the fluidic resistance of the system. The total electrical resistance of section 3 of the channel was estimated as $Z_3 = (Z_bL_b + Z_SL_S)n = [Z_hf_g + Z_S(1 - f_g)]L_3$. The predicted electrical resistance thus increases linearly with gas volume fraction f_g.

From the calculated resistance increase in section 3 and the experimental results for the resistance variation in the whole system, the streaming current in the chip channel past the T-junction I_{S3} could also be predicted using eqn (2) for both single phase flow and two-phase flow. The result is shown in Fig. 8(a). As can be seen, the streaming current in section 3 stays almost constant and equal to the value in single phase flow.

We now take the average value of I_{S3} (150 pA) (Fig. 8a) and the theoretically derived value for Z_3 as input for calculating the efficiency of section 3. To determine the efficiency of section 3, the input power for this section must be estimated. Sections 1 and 2 contain only water flowing at the measured flow rate Q_L, so that ΔP_1 and ΔP_2 can be computed. Assuming gas bubbles remain small (no bubble fusion) the pressure drop ΔP_4 in section 4 can be approximated by that of water flowing at a volumetric flow rate $Q_L + Q_g$. The pressure drop over section 3 could therefore be estimated as $\Delta P_3 = \Delta P_L - (\Delta P_1 + \Delta P_2 + \Delta P_4)$. The liquid and gas flow rates are the same as those for the entire system (Fig. 4), so that the input power P_{in3} can be estimated as $P_{in3} = \Delta P_3 Q_L + \Delta P_g Q_g$, with ΔP_g taken equal to the injection pressure P_g. By eqn (7), we could then estimate the efficiency in section 3 as $Eff = I_{S3}^2 Z_3/4P_{in3}$.

Taking a constant streaming current and an observed eight-fold increase of electrical resistance, we found that the total output power of section 3 was enhanced by 8 times with respect to single phase flow (Fig. 8b). Moreover, due to the increase of the pressure drop over section 3 and the decrease of the liquid flow rate, the input power decreases slightly. Hence, the maximum efficiency of section 3 will increase 11.3 times with respect to single phase flow (Fig. 8b inset).

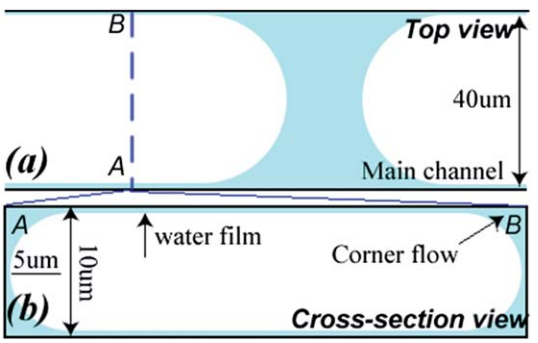

Fig. 6 A schematic (not to scale) of gas bubbles flowing in the main chip channel. Top view (a) and cross-section (b). The cross-sectional area of the liquid film near the wall can be ignored compared with the area of the liquid-filled corners.

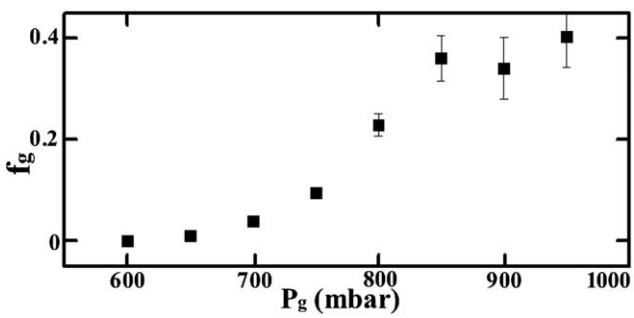

Fig. 7 Observed gas volume fraction f_g as a function of gas injection pressure P_g. Error bars indicate the inhomogeneous gas bubbles.

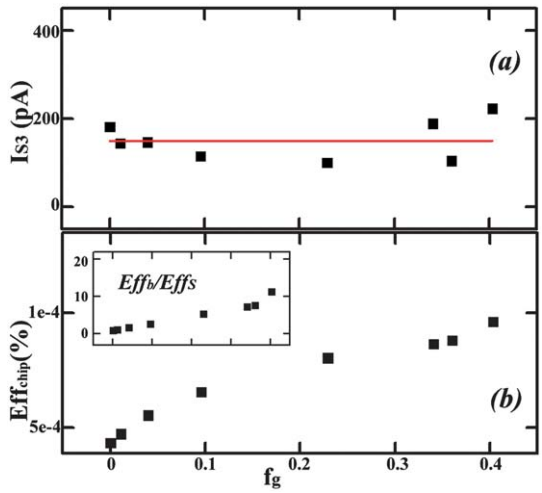

Fig. 8 (a) predicted streaming current I_{S3} in section 3 of the chip; the red line is a linear fit; (b) efficiency as a function of the gas injection pressure P_g; inset figure: efficiency ratio in section 3 (assuming a constant streaming current of 150 pA).

Discussion on efficiency

Though the absolute efficiency is strongly increased by the two phase flow, it is still very low in our system. There are several ways by which it might be increased. Methods adopted in single-phase flow are to reduce the salt concentration in the solution, thereby reducing its electrical conductivity, and to decrease the channel cross section.[21] An approach specific to our two-phase flow system would be to use cylindrical channels instead of rectangular ones. As shown in Fig. 6, in our chip the corners of the rectangular channels are always wetted by water, and provide a continuous path for electrical conduction even when the gas volume fraction is high. In a cylindrical channel the liquid film between the bubble and the capillary walls will be thin at low flow rates,[22] leaving only surface conductivity.[13] The electrical resistance Z_b will therefore be larger, as will be the maximum power output.

In conclusion, we successfully operated a two-phase flow streaming energy conversion system. Both the streaming current and the electrical resistance were increased by injecting gas bubbles and the output power and energy conversion were strongly enhanced.

References

1 S. Pennathur, J. C. T. Eijkel and A. van den Berg, *Lab Chip*, 2007, **7**, 1234–1237.
2 J. F. Osterle, *J. Appl. Mech*, 1964, **31**, 161.
3 W. Olthuis, B. Schippers, J. C. T. Eijkel and A. van den Berg, *Sens. Actuators, B*, 2005, **111–112**, 385–389.
4 J. Yang, F. Z. Lu, L. W. Kostiuk and D. Y. Kwok, *J. Micromech. Microeng.*, 2003, **13**(6), 963–970.
5 F. H. J. van der Heyden, D. J. Bonthuis, D. Stein, C. Meyer and C. Dekker, *Nano Lett.*, 2007, **7**(4), 1022–1025.
6 Y. B. Xie, X. W. Wang, J. M. Xue, K. Jin, L. Chen and Y. G. Wang, *Appl. Phys. Lett.*, 2008, **93**(16), 163116.
7 A. M. Duffin and R. J. Saykally, *J. Phys. Chem. C*, 2008, **112**(43), 17018–17022.
8 A. M. Duffin and R. J. Saykally, *J. Phys. Chem. C*, 2007, **111**(32), 12031–12037.
9 N. Linde, D. Jougnot, A. Revil, S. K. Matthai, T. Arora, D. Renard and C. Doussan, *Geophys. Res. Lett.*, 2007, **34**(3), L00306.
10 F. D. Morgan, E. R. Williams and T. R. Madden, *J. Geophys. Res.*, 1989, **94**(B9), 12449–12461.
11 P. Antraygues and M. Aubert, *J. Geophys. Res.*, 1993, **98**(B12), 22273–22281.
12 A. Revil and A. Cerepi, *Geophys. Res. Lett.*, 2004, **31**(11), L11605.
13 J. D. Sherwood, *Langmuir*, 2008, **24**(18), 10011–10018.
14 J. D. Sherwood and E. Lac, *J. Colloid Interface Sci.*, 2010, **349**(1), 417–423.
15 J. D. Sherwood, *Phys. Fluids*, 2007, **19**(5), 053101.
16 H. Daiguji, P. D. Yang, A. J. Szeri and A. Majumdar, *Nano Lett.*, 2004, **4**(12), 2315–2321.
17 A. Malhotra and J. N. Coupland, *Food Hydrocolloids*, 2004, **18**, 101–108.
18 H. M. Fagerholm, C. Lindsjö and J. B. Rosenholm, *J. Mater. Sci.*, 1995, **30**, 2420–2424.
19 S. A. Vanapalli, A. G. Banpurkar, D. van den Ende, M. H. G. Duits and F. Mugele, *Lab Chip*, 2009, **9**(7), 982–990.
20 E. Oosterbroek, *Modeling, Design and Realization of Microfluidic Components*, PhD Thesis, University of Twente, 1999
21 D. Stein, M. Kruithof and C. Dekker, *Phys. Rev. Lett.*, 2004, **93**, 035901.
22 F. P. Bretherton, *J. Fluid Mech.*, 1961, **10**, 166–188.